*Q. J. R. Meteorol. Soc.* (2001), **127**, pp. 1893–1916

# Observations of atmosphere–ocean coupling in the North Atlantic

By ARNAUD CZAJA* and JOHN MARSHALL
*Massachusetts Institute of Technology, USA*

(Received 28 December 2000; revised 6 April 2001)

SUMMARY

An index of sea surface temperature (SST) variability, $\Delta T$, is introduced that measures the difference in SST across the separated Gulf Stream in late winter. By analysing a long observational record of SST and sea-level pressure (SLP), it is shown that $\Delta T$ exhibits damped oscillations of decadal period, and covaries with the strength of a dipolar SLP anomaly reminiscent of the North Atlantic Oscillation (NAO). Analysis in the frequency domain shows a broad-band 'peak' at 10–20 years in $\Delta T$, with a continuous decrease of power on longer time-scales. Similar spectral signatures are found in the northern part of the SLP dipole (the Greenland–Icelandic Low region) but not in its southern part (the subtropical High region), whose power increases on long time-scales.

The observations are interpreted in the framework of a delayed-oscillator model in which the ocean circulation introduces the delay, and modulates $\Delta T$ on decadal time-scales. The decrease of power seen on long time-scales (>25 years) in the $\Delta T$ index is captured by a model including wind-driven ocean circulation, and arises primarily as a passive response of the latter to the NAO forcing. Variability of the ocean's meridional overturning circulation could also play a role in modulating $\Delta T$ on decadal time-scales. If a small feedback of $\Delta T$ on the NAO pattern is introduced, the simple model can also reproduce the spectral structures seen in the SLP anomaly in the Greenland–Iceland region.

KEYWORDS: Air–sea interaction Decadal climate variability North Atlantic Oscillation

## 1. INTRODUCTION

Year-to-year fluctuations in the path and strength of North Atlantic storms induce large-scale sea surface temperature (SST) anomalies. Short time-scale variations in SST (a year or so) are a response to local fluctuations in surface heat exchange, primarily driven by stochastic atmospheric variability (Cayan 1992; Battisti *et al.* 1995). However, as one approaches the western boundary of the North Atlantic basin, advection of heat by ocean currents can play a role in modulating SST on longer time-scales (Bjerknes 1964; Halliwell 1998), and may potentially impact the climate. Deser and Blackmon (1993), on the basis of an empirical orthogonal function (EOF) analysis of surface climate variables in winter (1900–89), have isolated a large-scale SST pattern whose power spectrum shows a broad-band peak near the decadal period. The SST pattern shows anomalies of opposite sign roughly north and south of the mean position of the separated Gulf Stream, extending to the eastern subtropics in the form of a tripolar SST pattern. The associated surface atmospheric circulation is reminiscent of the North Atlantic Oscillation (hereafter the NAO), and similarly exhibits enhanced power at the decadal period. These findings have been confirmed by Sutton and Allen (1997) and others (e.g. Mann and Park 1994; Tourre *et al.* 1999). Sutton and Allen (1997) in particular, using SST and sea-level pressure (SLP) data since the early 1950s to the present, also find suggestions of propagation of SST anomalies along the path of the extended Gulf Stream.

Although Deser and Blackmon (1993) have suggested that the decadal time-scale may be due to changes in the thermohaline oceanic circulation, there is not yet a consensus on the mechanisms governing the low-frequency evolution of the SST 'tripole'. Grötzner *et al.* (1998) have argued that it may reflect an interaction between the NAO and the wind-driven ocean circulation, as suggested by analysis of extended integrations

* Corresponding author: Department of Earth, Atmospheric and Planetary Sciences, Room 54 - 1421, Massachusetts Institute of Technology, 77 Massachusetts Avenue, Cambridge, MA 02139, USA.
e-mail: czaja@ocean.mit.edu

of a coupled atmosphere–ocean model. The lack of long observational records of subsurface oceanic data is clearly a limiting factor in evaluating the role of the ocean circulation in the decadal variability seen at the surface. Also, many studies lack a theoretical framework to guide analysis of the observations. The interpretation of the results is made even more difficult by the use of complex and elaborate statistical techniques (EOFs, principal oscillation patterns—see Grötzner *et al.* (1998), and multivariate frequency domain methods like the MTM-SVD of Mann and Park (1994)).

Here, to explore evidence and possible mechanisms of atmosphere–ocean coupling, in section 3 we introduce and study a simple SST index, $\Delta T$, from a long observational record (1856–1998); it measures the strength of the dipole of SST that straddles the Gulf Stream. Pronounced decadal signals in $\Delta T$ are found which, as shown in section 4, covary with the strength of SLP anomalies over the Greenland–Iceland Low and subtropical High regions. Using the simple coupled model developed by Marshall *et al.* (2001a), in section 5 we interpret features of the power spectrum of observed SST and SLP as the signature of coupled interactions between the atmospheric and oceanic circulations over the North Atlantic. A comparison with previous studies is offered in section 6, and the conclusions are presented in section 7.

## 2. Data and method

The SST and SLP anomalies used in this study come from the 'optimal analysis' of historical datasets made by Kaplan and collaborators (Kaplan *et al.* (2000) for SLP; Kaplan *et al.* (1997) for SST). Anomalies are defined with respect to a climatological annual cycle formed over the 1951–80 period, extending in time from 1855 to 1992 for SLP and from 1856 to 1999 for SST. The spatial resolution of the data is 5° for SST and 4° for SLP. Only anomalies north of 30°S have been considered. The raw data used in the study were obtained from the Lamont–Doherty Earth Observatory website*, and were linearly detrended before analysis. No filtering or smoothing of any kind has been subsequently applied to the data. Some products of the NCEP–NCAR† reanalysis (Kalnay *et al.* 1996) will also be used.

Much use will be made of power spectra; they are computed using the multitaper method (Percival and Walden 1993), with the number of tapers $K$ set to $K = 7$. Upper and lower error bars on the power spectrum will be estimated according to a $\chi^2_\nu$ test, with the number of degrees of freedom $\nu = 2K$ (Percival and Walden 1993). Cross-spectral analysis will also be employed, with a Daniell window for reducing the variance of the spectral estimate and a cosine taper window to reduce spectral leakage. The smoothing parameter $M$ of the Daniell window is set to either $M = 5$ or $M = 6$, as indicated in the text. The value at which the squared coherence is significantly different from zero at the 95% confidence level is estimated following Amos and Koopmans (1963).

## 3. A middle latitude SST index

### (a) *Index time series*

We focus on late winter (February, March, April), when the ocean mixed layer has built large thermal anomalies in response to wintertime storms. A late-winter SST index was constructed by taking the difference of the SST anomaly averaged over boxes north ($T_N$) and south ($T_S$) of the separated Gulf-Stream, as indicated in Fig. 1. The path of the Gulf Stream is coincident with the region of enhanced SST gradients along the

* URL http://ingrid.ldeo.columbia.edu/SOURCES/.KAPLAN

† National Centers for Environmental Prediction–National Center for Atmospheric Research.

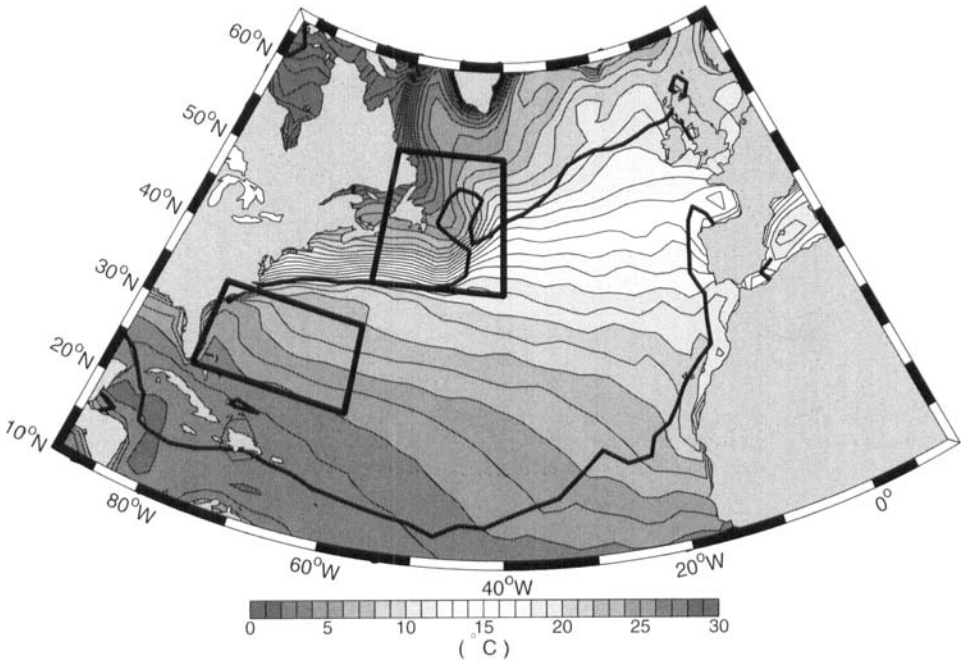


Figure 1. Annual mean sea surface temperature (SST) (grey shading) and position of the zero wind-stress-curl line (thick black lines) from the NCEP climatology (1961–90). The two black boxes indicate the regions used to construct the dipole SST index $\Delta T = T_N - T_S$, where $T_N$ is the temperature in the northern box and $T_S$ the temperature in the southern box.

climatological zero wind-curl line evident in the mean SST, Fig. 1 grey shading. This particular index, $\Delta T = T_N - T_S$, was chosen because:

(i) it is a measure of low-level baroclinicity to which cyclogenesis at the beginning of the Atlantic storm-track may be sensitive, and

(ii) it may repsond to anomalies in ocean heat transport associated with both wind-driven gyres and thermohaline circulation.

Note that the southern box ($T_S$) is almost coincident with the 'storm formation region', as defined by Sutton and Allen (1997).

The time evolution of $\Delta T$ can be seen in Fig. 2. Typical $\Delta T$ anomalies are found to be of order 1 K on interannual time-scales (raw data) and 0.5 K at lower frequencies (low-pass time series). The last 60 years or so of the low-pass record show 'decadal oscillations' whereas the first half of the record suggests a pronounced downward trend from 1890 to 1920. We note some similarity in the time evolution of our $\Delta T$ index and the second principal component of wintertime SST found by Deser and Blackmon (1993). This is to be expected from our definition of $\Delta T$ and the pattern of this principal component, which has dipolar SST anomalies straddling the separated Gulf Stream (see introduction). However, the upward trend between 1920–50 and the subsequent fall seen in Deser and Blackmon (the second principal component time series shown in their Fig. 1(d)) is less pronounced in $\Delta T$.

### (*b*) *Associated large-scale SST patterns*

To determine the large-scale SST pattern captured by our index we constructed composite maps of SST anomalies north of the equator based on $\Delta T$ (Fig. 3). These are

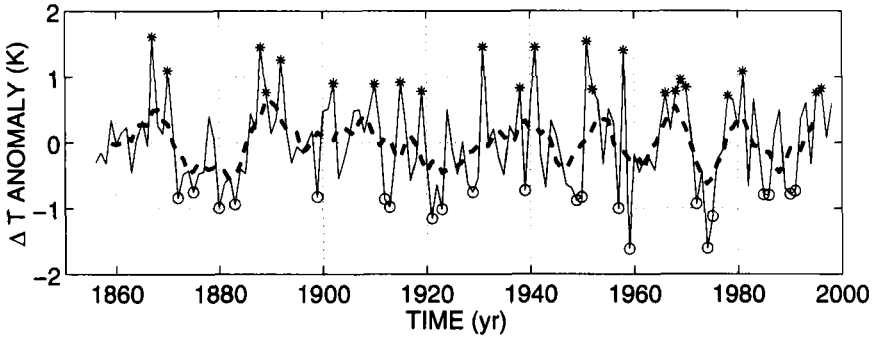


Figure 2. Late winter (averaged from February through April) time series of $\Delta T$ (see text). The continuous curve is the raw yearly data while the dashed curve indicates a 6-year running mean. Stars and circles denote the years retained to construct the composite maps shown in Fig. 3.

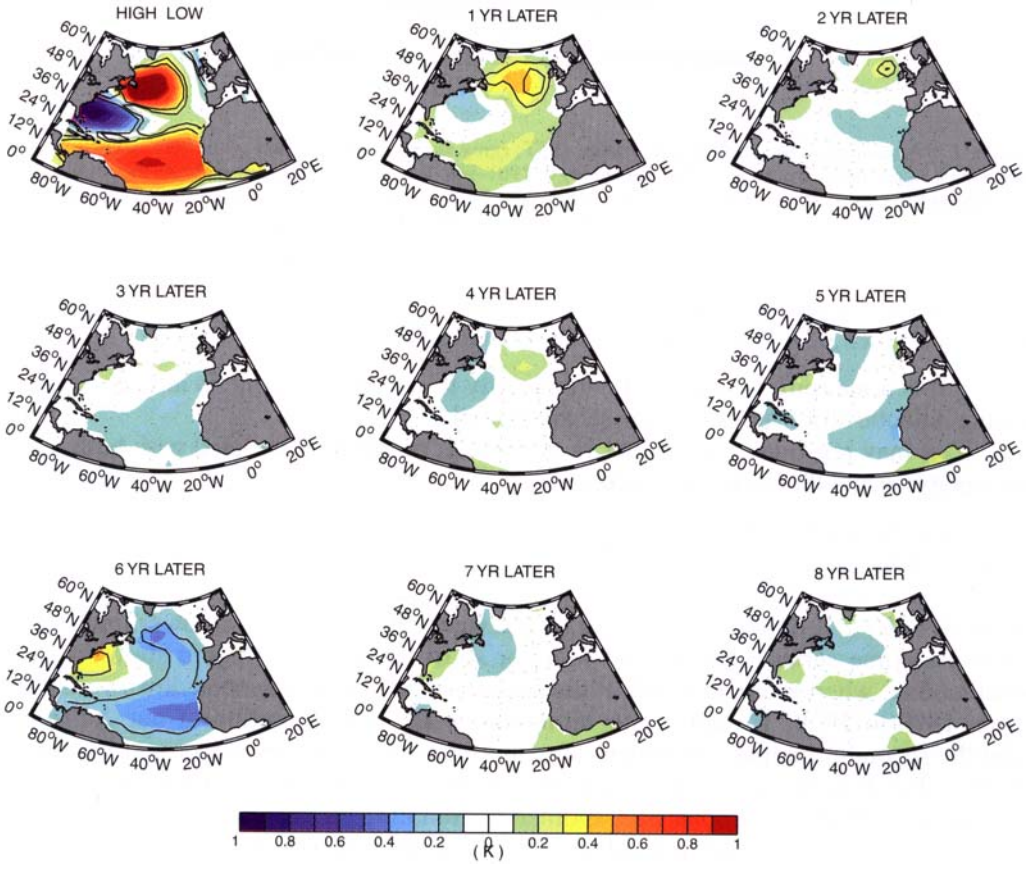


Figure 3. Composite maps of sea surface temperature anomalies (K) based on years in which $|\Delta T| > 0.7$ K (indicated by stars and circles in Fig. 2). The 'high − low' map is obtained by substracting the high-index composite from the low-index composite. The '1-year later' map is obtained by substracting the high index +1-year composite from the low index +1-year composite. The black lines indicate the 95 and 99% confidence levels estimated from a Student's $t$-test, assuming 6 (warm independent $\Delta T$ years) + 6 (cold independent $\Delta T$ years) − 2 = 10 degrees of freedom.

difference maps between average conditions during warm ($\Delta T$ high and positive, stars in Fig. 2) and cold ($\Delta T$ low and negative, circles in Fig. 2) time intervals. The result is shown at the top left panel of Fig. 3 and represents the typical amplitude of SST anomalies in the North Atlantic associated with the transition from $\Delta T > 0$ to $\Delta T < 0$. It is very similar to the dominant pattern of SST variability over the North Atlantic in winter—the 'tripole' (see introduction)—with positive correlation between SST anomalies over the subtropics and north of the separated Gulf Stream. The composite pattern explains 30% of the SST variance in late winter. It is primarily a result of the local surface forcing (turbulent surface heat flux, entrainment at the bottom of the mixed layer, Ekman advection) orchestrated by the dominant mode of atmospheric variability over the Atlantic sector, the NAO (Cayan 1992; see also section 4(a)).

Composites can also be used to reveal the typical time evolution of large-scale SST anomalies associated with $\Delta T$ by shifting the years used to form them relative to those represented by the stars and circles in Fig. 2. We find indication for a slight persistence of the large-scale tripolar SST pattern one year after it has been generated (Fig. 3, 1 year later), but this signal is lost 2 years later, as would be expected if the ocean had no memory other than that due to the thermal inertia of the mixed layer*. Strikingly, however, the SST pattern reappears after 6 years, but with opposite sign (Fig. 3, 6 years later). This suggests that the ocean is responding to the atmospheric surface forcing on a longer time-scale than the fast local adjustment of its mixed layer revealed by the zero-lag composite (Fig. 3, high – low). Analysis of the composites at longer lags suggests a reappearance of the initial tripole 14 years after high and low $\Delta T$ events, but the signal is not statistically significant (not shown).

This simple composite analysis thus reveals a complex time and spatial evolution of SST anomalies associated with $\Delta T$. In contrast with the canonical stochastic climate model which would predict an exponential decay of the large-scale SST pattern (Frankignoul and Hasselman 1977 (hereafter FH77); see section 5), there is evidence of damped oscillatory behaviour.

### (*c*) *Spectral analysis*

Analysis of the frequency content of the $\Delta T$ index is shown in Fig. 4. We first separately analysed the power spectrum of $T_N$ and $T_S$. As a reference we superimposed the power of a first-order Markov process with the same 1-year autocorrelation and variance as the raw data (Box *et al.* 1994). In the following, this will be referred to as the 'equivalent' AR(1) process.

One sees departures from the equivalent AR(1) at interdecadal periods for $T_N$ and at decadal and interannual periods for $T_S$. The power spectrum of their difference $\Delta T = T_N - T_S$ (Fig. 4) has even more structure, with a pronounced increase of variance near the 10 to 20-year band and decrease of power at lower frequency. This contrasts sharply with the power spectrum of its equivalent AR(1) process. Figure 4 also indicates the presence of other spectral structures in the $\Delta T$ index at higher frequencies (3 to 5-year band, and 2 to 3-year band), which will not be addressed here.

Direct cross-spectral analysis between $T_N$ and $T_S$ (Fig. 5) shows that they are out of phase over a broad range of frequencies, with significant squared coherence at decadal ($\simeq$0.1 cycles per year (cpy)) and interannual (0.2–0.4 cpy) periods. A particularly high squared coherence is found in the 10 to 15-year band, where, remarkably, it is higher than that found at interannual periods. Such a frequency dependence is striking and

* Frankignoul *et al.* (1998) (see also Czaja and Frankignoul (1999)) have estimated the turbulent heat flux feedback over the North Atlantic and found it damps SST anomalies at a rate $\simeq$20 W m$^{-2}$K$^{-1}$. This is a damping time-scale $\simeq$8 months for a mixed layer of depth 100 m.

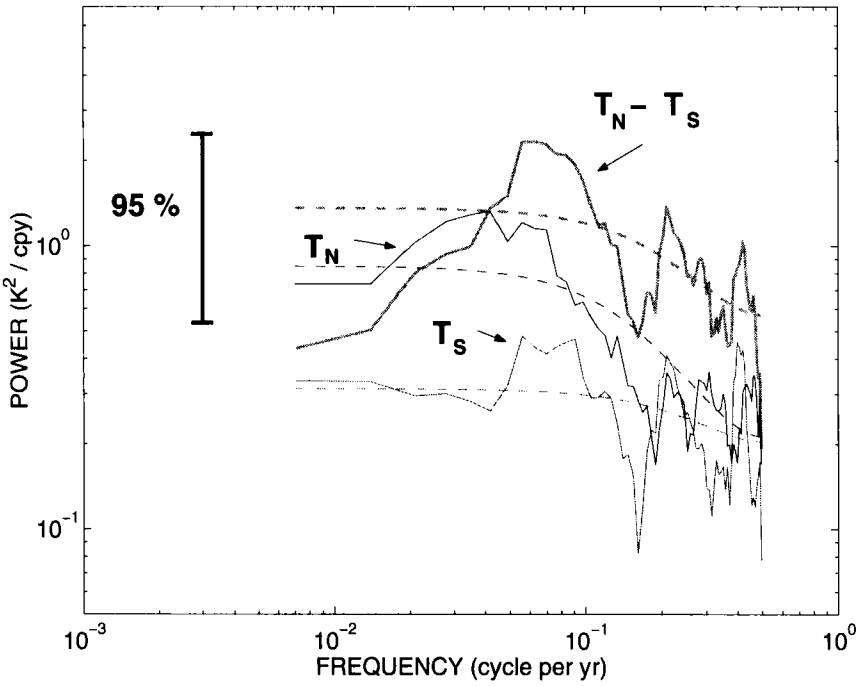


Figure 4. Power spectra of $T_S$, $T_N$ and their difference $\Delta T$ (see text) in late winter. The dashed lines indicate the power of their equivalent AR(1) process (see text, section 3(c)). The 95% confidence level is indicated by the black vertical line.

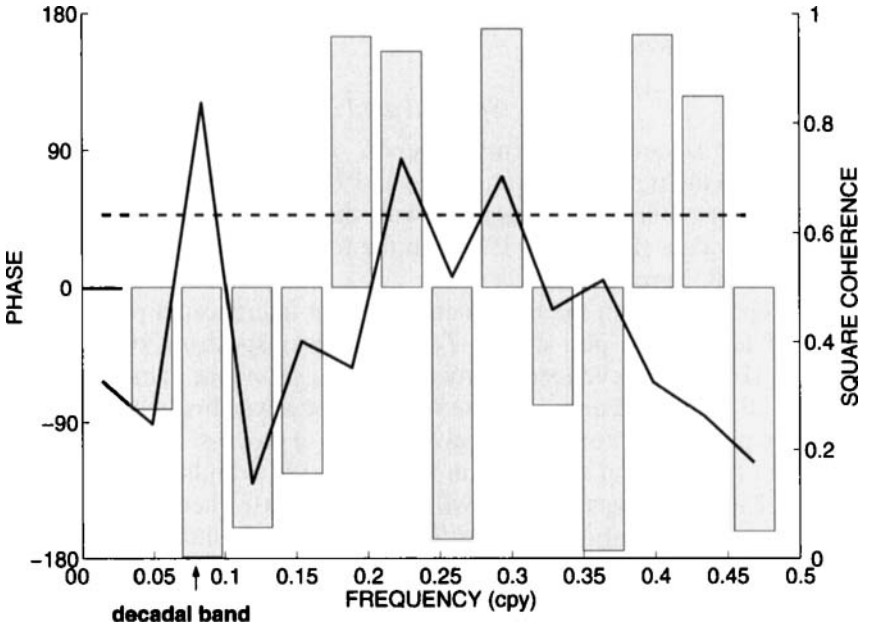


Figure 5. Phase spectrum (bars, in degrees as indicated on the left $y$-axis) and squared coherence (thick curve, right $y$-axis) between $T_N$ and $T_S$ (see text) as a function of frequency (in cycles per year). The width of the Daniell window $M$ has been set to 5, and the corresponding level of significance for the squared coherence at the 95% level is indicated as the dashed horizontal line (see section 2).

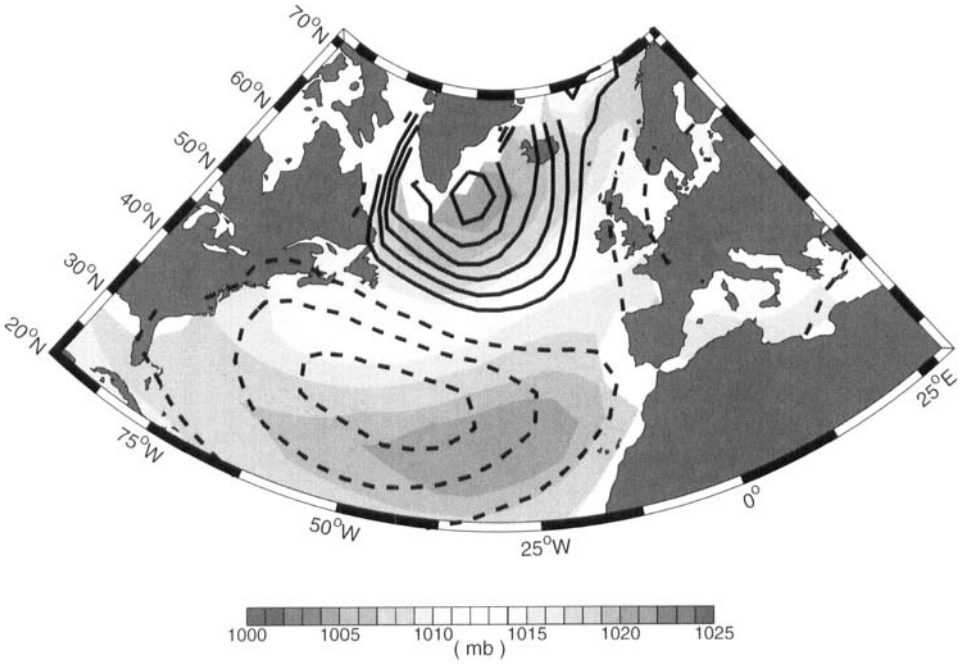


Figure 6. Composite of sea level pressure (SLP) anomalies (contour interval 1 mb, negative values shown dashed) for 'high − low' $\Delta T$ years (see text). The COADS mean SLP in late winter is plotted in grey shading. The same warm and cold $\Delta T$ years have been used as in Fig. 3 (high − low).

suggests that there is an efficient mechanism in the 10 to 15-year band which modulates SST anomalies in the vicinity of the Gulf Stream with opposite effects north and south of its mean separation path. We will argue in sections 4 and 5 that an anomalous wind-driven oceanic gyre may transport heat from the southern ($T_S$) to the northern ($T_N$) box, providing a possible mechanism. Advection of heat by anomalies in the meridional overturning circulation may also play a role—see Marshall *et al.* (2001a).

## 4. Sea-level-pressure anomalies covarying with $\Delta T$

### (*a*) *Composite analysis*

We now study the atmospheric conditions associated with $\Delta T$, as revealed by SLP anomalies. The spatial pattern of late winter (February through April) SLP anomalies characterizing the difference of average conditions between warm ($\Delta T > 0$) and cold ($\Delta T < 0$) years is contoured in Fig. 6. It is the SLP analogue of the SST composite shown in Fig. 3 (high − low, upper left panel). The composite was constructed using SLP data down to 30°S but significant anomalies were only found north of the equator (not shown). The composite explains 25% of the late winter SLP variance. In Fig. 6, the contours refer to the composite values whereas the grey shading indicates the mean SLP in late winter from the Comprehensive Ocean–Atmosphere Data Set (COADS).

We see that the northern and southern centres of action of the SLP pattern shown in Fig. 6 project strongly on the mean SLP pressure map, so that in positive $\Delta T$ years the surface westerlies and the trade winds are weakened. There is also a hint of negative pressure anomalies over western Europe, but this is poorly sampled by the Kaplan analysis which only uses surface marine observations. It may indicate a more zonal path of the storms during warm $\Delta T$ years.

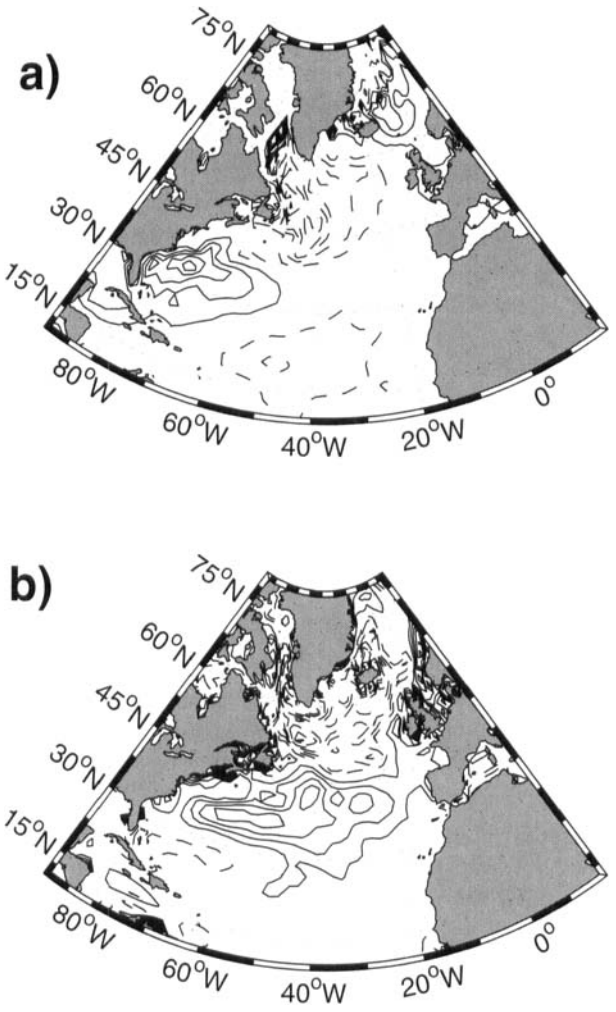


Figure 7. Maps of (a) surface turbulent heat flux (latent + sensible, contour interval 5 W $m^{-2}$, dashed for negative) and (b) surface wind-stress-curl anomalies (contour interval $10^{-8}$ N $m^{-3}$, dashed for negative) regressed onto the $\Delta T$ index (see text) in late winter. The surface heat flux (wind-stress curl) is positive upward (cyclonic). The maps give the typical changes in heat flux and wind-stress curl associated with one standard deviation of the $\Delta T$ index. All data come from the NCEP–NCAR reanalysis over the period 1958–98.

(i) *Fast oceanic response to the SLP changes.* In agreement with Cayan (1992), we note that the dipolar SLP pattern shown in Fig. 6 is very likely to generate locally the SST pattern shown in Fig. 3 (high − low). Weakening of the north-westerly winds over the Labrador Sea and the trades leads to a reduction in the turbulent surface heat flux in these regions, thereby explaining, at least qualitatively, the positive lobes seen in Fig. 3 (high − low). Conversely, anomalous advection of dry continental air by the anomalous cyclone seen in Fig. 6 is likely to induce the negative SST anomalies observed to the south of the separated Gulf Stream in Fig. 3 (high − low). The regression map of anomalous surface turbulent heat flux (latent + sensible) from the NCEP–NCAR reanalysis onto $\Delta T$ supports these inferences (Fig. 7(a)). Anomalous Ekman transport is also likely to play a role in the generation of this large-scale SST pattern (not shown). We are thus led to interpret the combined SST–SLP composite for high − low $\Delta T$

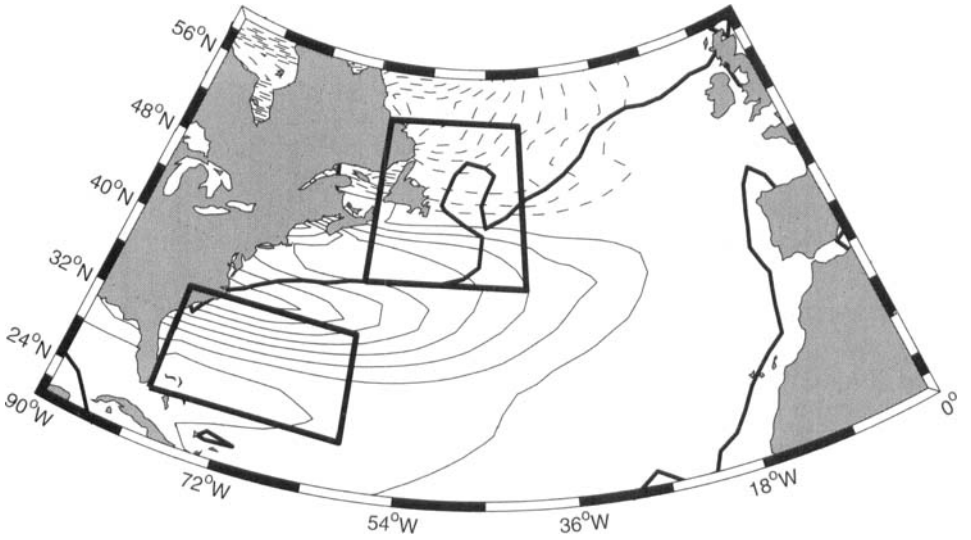


Figure 8. Anomalous geostrophic transport (positive—i.e. anticyclonic—stream function contoured as continuous lines, every Sv, i.e. $10^6$ $m^3s^{-1}$), inferred from the application of Eq. (1) (with $x_E = 10°W$) and using the surface wind-stress-curl anomalies shown in Fig. 7(b) (but with opposite signs). The climatological mean position of the zero wind-stress-curl line is indicated by the thick black line. The two black boxes indicate the regions used to define the $\Delta T$ index (see text).

index conditions (Fig. 3, high − low; Fig. 6) as reflecting a passive ocean response to the surface forcing orchestrated by the SLP composite.

(ii) *Slow oceanic response to the SLP changes.* The ocean circulation will also adjust to the strengthening/weakening of the atmospheric surface winds associated with the SLP composite. We show, in Fig. 7(b), the regression of the surface wind-stress-curl anomalies onto $\Delta T$. In agreement with the SLP composite, it is found that in years when $\Delta T > 0$, there is a weakening of the anticyclonic (cyclonic) surface wind stress over the subtropical (subpolar) gyre. Conversely, years when $\Delta T < 0$ are associated with an enhanced anticyclonic (cyclonic) wind-stress forcing over the subtropical (subpolar) gyres.

We can estimate the equilibrium response of the ocean circulation to this mechanical forcing using linear Sverdrup dynamics. Denoting the depth-integrated stream function of the geostrophic response by $\Psi$, at equilibrium we have

$$\Psi(x, \phi) = -\frac{a \tan \phi}{\rho_0} \int_{x_E}^{x} \mathbf{k} \cdot \left( \nabla \times \frac{\tau}{f_{Cor}} \right) dx' \tag{1}$$

where $\mathbf{k}$ is the vertical unit vector, $\tau$ denotes the wind-stress pattern obtained by linear regression of the surface wind anomalies onto the $\Delta T$ index, $\phi$ is latitude, $x$ longitude ($x_E$ is the longitude of the eastern boundary where we assume $\Psi(x_E, \phi) = 0$), $f_{Cor}$ the Coriolis parameter at latitude $\phi$, $a$ is the radius of the earth, and $\rho_0$ is the density of sea water. The resulting Sverdrup flow is shown in Fig. 8. We observe an anomalous circulation straddling the climatological subtropical and subpolar gyres, whose separation is delineated as the climatological position of the zero wind-stress-curl line (Fig. 8). It is assumed that this circulation is closed by a western boundary current, which is not modelled by (1). The maximum transport of this 'intergyre' gyre (see Marshall *et al.* (2001a)) occurs close to the separation point of the Gulf Stream, near

Cape Hatterras. The circulation shown in Fig. 8 has a typical amplitude of about 8 Sv, which results from the typical wind-stress-curl changes associated with one standard deviation of $\Delta T$ (Fig. 7(b)). This basic pattern will be stochastically forced by the overlying atmosphere and, in a 1st baroclinic mode ocean, will be spun up at the time it takes a 1st baroclinic Rossby wave to cross the basin, about 5 to 10 years depending on latitude (see section 5(a)).

As shown in appendix A, the heat transport of the intergyre gyre across the mean separated Gulf Stream is comparable in magnitude with the total heat delivered at the surface over the $T_N$ and $T_S$ boxes on decadal time-scales. We find that the heat transport of the intergyre gyre across the ocean mixed layer is $\sim$25 TW (1 TW $= 10^{12}$ W), whilst the regression of the NCEP–NCAR turbulent heat fluxes onto $\Delta T$ suggests typical changes of about 10 $\mathrm{Wm}^{-2}$ over the northern and southern boxes on decadal time-scales (not shown), i.e. a total heat input of $\simeq$40 TW (assuming a typical box area of $4 \times 10^{12}$ $\mathrm{m}^2$). On time-scales longer than about 25 years, we predict that the impact of the intergyre gyre on $\Delta T$ opposes the local forcing by air–sea heat fluxes. Once the intergyre gyre is spun up and, following years when the atmospheric circulation is strengthened, circulates anticyclonically, it transports heat from the southern to the northern side of the Gulf Stream (see Marshall *et al.* (2001a)). Since the strengthening of the atmospheric circulation locally generates colder SST to the north and warmer SST to the south of the separated Gulf Stream axis, the intergyre gyre acts to reduce, with some delay, the anomalous SST gradient across the Gulf Stream.

As will be shown in section 5, incorporating anomalous advection of heat by the intergyre gyre (a $v'\overline{T}$ term) can successfully reproduce the time behaviour of the observed $\Delta T$ index, assuming a plausible Rossby wave transient time of $\simeq$10 years. However, such a mechanism does not explain the simultaneous change of sign of SST anomalies observed in the subtropics, 6 years after they have been generated (Fig. 3). It can be argued that the NAO is sensitive to $\Delta T$, and that the decadal signal seen in the Gulf Stream region can be communicated to the subtropics via an 'atmospheric bridge'. Ocean circulation and possible coupling between $\Delta T$ and the NAO are essential features of the model we will use in section 5 to interpret the observations.

### (*b*) *Co-spectral analysis*

(i) *Interannual to decadal time-scales.* We investigate the frequency dependence of the relationship between $\Delta T$ and the SLP composite in Fig. 9, which shows the cross-spectrum (squared coherence and phase) of the $\Delta T$ and SLP anomaly averaged over the zonal band 50°–20°W. It is seen that, at both interannual and decadal time-scales, the squared coherence is maximum in the zones 20°–30°N and 50°–60°N, i.e. near the Greenland–Iceland Low (hereafter GIL) and the subtropical High (hereafter STH) regions. The $\Delta T$ index is found in phase with the GIL and out of phase with the STH (Fig. 9). Thus the association between $\Delta T$ and the dipolar SLP anomaly seen in Fig. 6 is found over a broad range of frequencies, up to the 12 to 25-year band (see below for longer time-scales).

The strength of the SLP dipole (GIL − STH) is tested as a function of frequency in Fig. 10. It is seen that the squared coherence remains high between the GIL and SLP anomaly near 20°–30°N, being slightly stronger at interannual ($\simeq$0.85) than at decadal ($\simeq$0.7) time-scales. The phase is stable, with an out-of-phase relationship between the GIL and SLP anomaly over the STH region at all frequencies. One notes the tendency for the maximum squared coherence in the STH region to move southward on longer time-scales: it is located near 30°N in the interannual band, but is found near 20°N

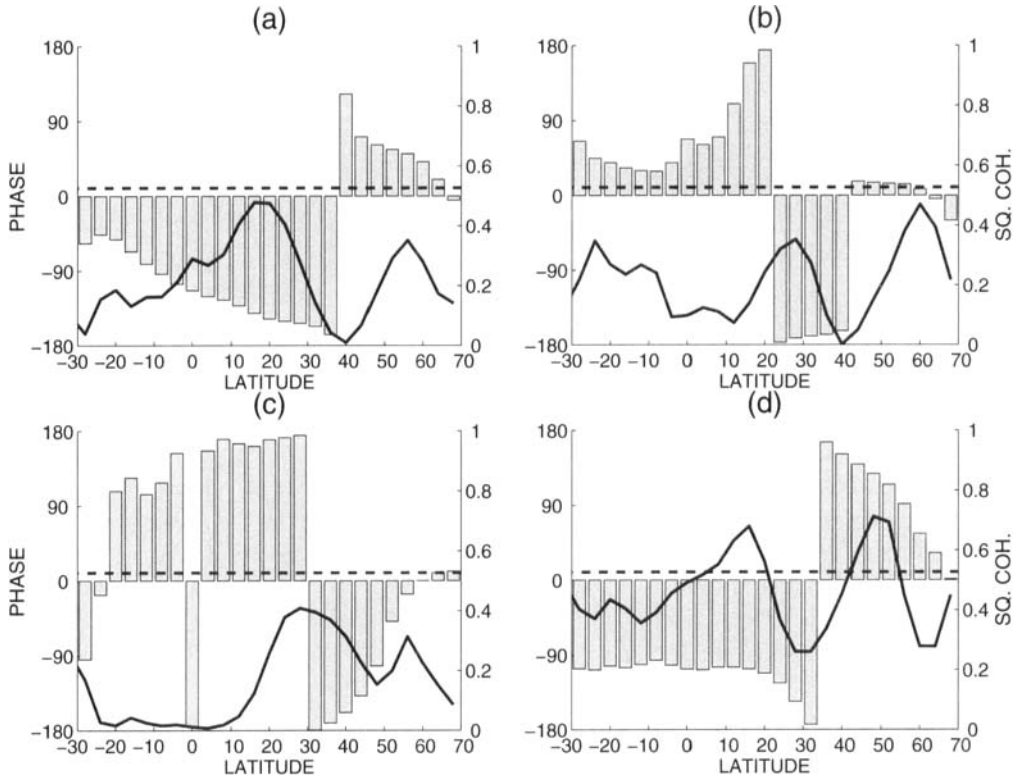


Figure 9. Phase (bars, in degrees as indicated on the left $y$-axis) and squared coherence (thick curve, right $y$-axis) between $\Delta T$ (see text) and the sea level pressure (SLP) anomaly (averaged over the 50°–20°W zonal band) for (a) 12–25, (b) 8–12, (c) 6–8 and (d) 4–5 years (the Daniell window parameter $M$ is set to $M = 6$). The 95% confidence level for the squared coherence is indicated as the dashed horizontal line.

in the decadal band. This shift indicates that the nodal line separating the dipolar SLP anomaly over the Atlantic is not fixed at a given latitude (as perhaps is suggested by an EOF analysis) but fluctuates in time.

(ii) *Longer time-scales.* We show in Fig. 11 the power spectrum of the late winter (February through April) GIL and STH indices. On periods shorter than about 20 years (frequencies > 0.05 cpy), there is a close similarity between these spectra, as expected from the strong coherence displayed by these indices at these time-scales (see Fig. 10). On longer time-scales, however, we see distinct structures in the power spectrum. In the STH region, the power is clearly reminiscent of that of the NAO index of Hurrell (1995; also indicated in Fig. 11), with increasing power with time-scales. Interestingly, the GIL power spectrum has an opposite trend on time-scales longer than about 20 years, which accordingly reveals a broad-band peak near 10–20 years.

Because of the particular treatment of the very long time-scales in the Kaplan *et al.* (2000) analysis (see the discussion by Hurrell and Trenberth (1999)), we have recomputed the power spectra of the GIL and STH with the Trenberth and Paolino (1980) dataset, and found very similar results (not shown). We note also that the spectra are not sensitive to the technique used to estimate them. We have checked that other techniques, such as the simple averaged periodogram, give the same SLP spectra as that obtained using the multitaper method. The low-frequency structures in the GIL and STH spectra are thus robust.

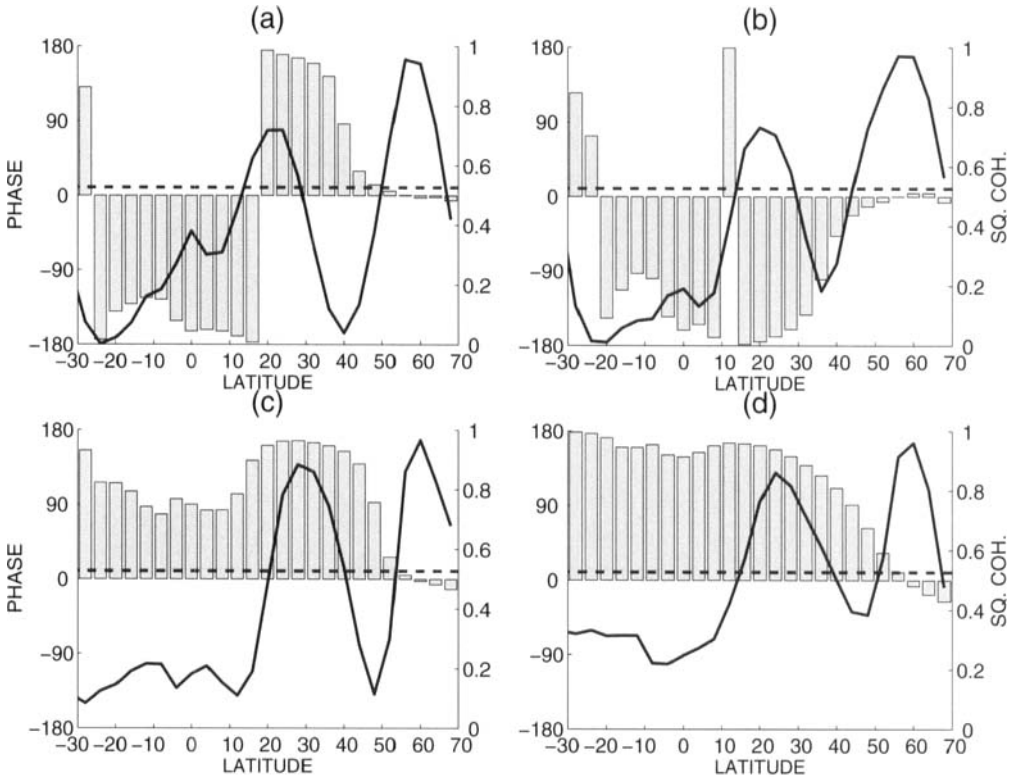


Figure 10. Same as Fig. 9 but for the Greenland-Iceland Low instead of $\Delta T$.

The similarity of the $\Delta T$ and GIL power spectra is striking. We showed in the previous section that these indices remain coherent on interannual to decadal time-scales. Figure 12 shows the spectral coherence of $\Delta T$ with the 'zonally' (50°–20°W) averaged SLP field on time-scales longer than 25 years (the first frequency band obtained using a Daniell window with $M = 6$). We see that the coherence between $\Delta T$ and SLP remains strong at these long time-scales, particularly in the vicinity of 50°N where they are in phase (Fig. 12). Thus, as the power of $\Delta T$ decreases on long time-scales, so does that of the GIL, with both indices remaining coherent (they share more than 50% of their variance at time-scales longer than 25 years, according to Fig. 12).

The observed decrease of power of $\Delta T$ and GIL is atypical of midlatitude SST and SLP spectra. More frequently, such spectra either tend to flatten at long time-scales (as seen in many modelling studies—see for instance Saravanan *et al.* (2000)), or slightly increase with time-scales, as seen in Hurrell's NAO power spectrum or the first EOF of North Atlantic SST presented in the recent review by Marshall *et al.* (2001b). In section 5, we will argue that the broad peak in the $\Delta T$ and SLP spectra is consistent with the expected role of the ocean circulation, which, at long time-scales, acts as an additional damping on $\Delta T$. Because the decrease of power at low frequencies is not only seen in $\Delta T$ but also in the GIL, with both indices remaining coherent on long time-scales, we suggest that the observations may reflect evidence for a coupled atmosphere–ocean mode of variability over the North Atlantic. It will be shown that only a modest feedback of $\Delta T$ on the NAO is required to reproduce the observed SLP and SST spectra.

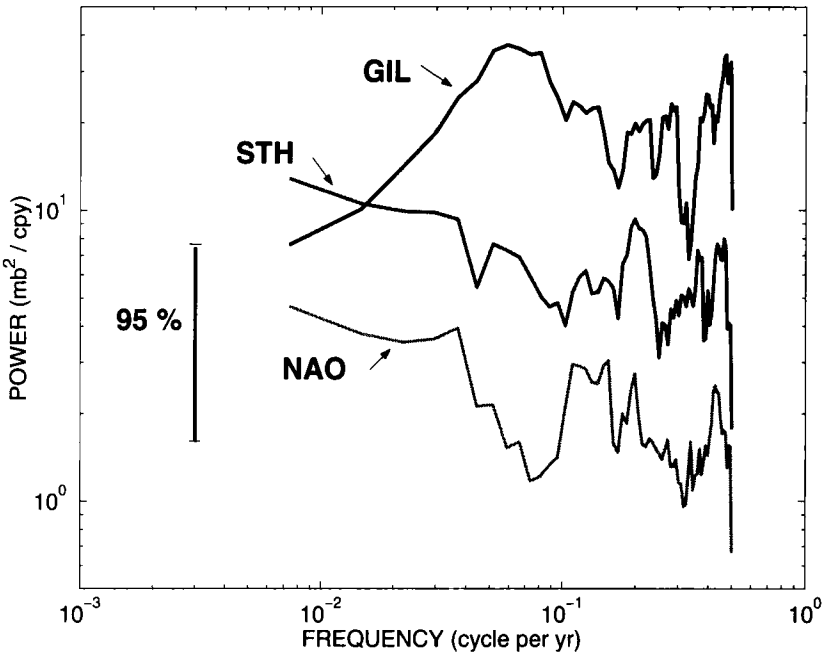


Figure 11. Same as Fig. 4 but for the Greenland–Iceland Low (GIL), sea level pressure (SLP) anomaly averaged over 50°–20°W/50°–70°N), Subtropical High (STH) SLP anomaly averaged over 50°–20°W/20°–40°N), and the North Atlantic Oscillation (NAO) index of Hurrell (1995). The power of the NAO is dimensionless (the time series has been normalized by its standard deviation).

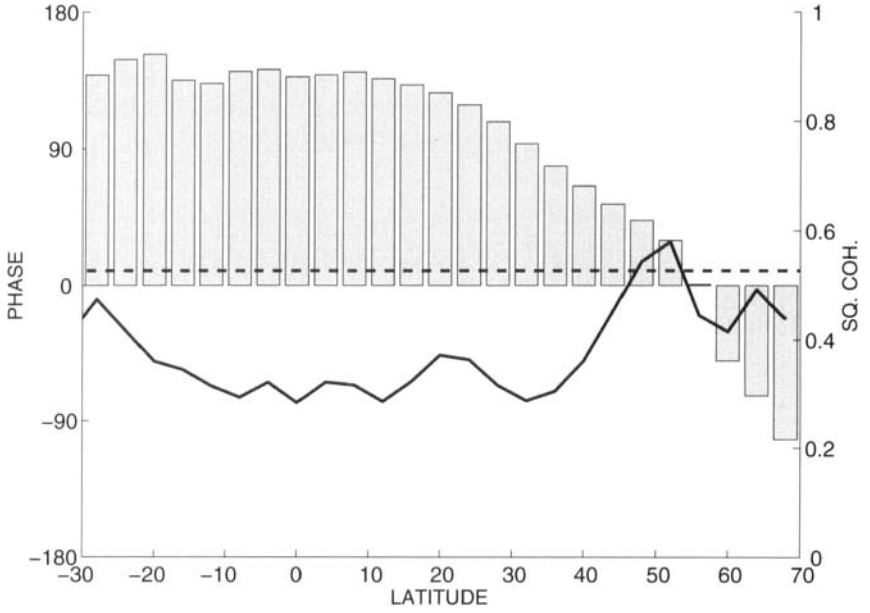


Figure 12. Same as Fig. 9 but for time-scales longer than 25 years.

(iii) *Seasonal dependence of the $\Delta T$ and GIL spectra.* We repeated the spectral analysis on the GIL and $\Delta T$ for seasons other than the late-winter period. We found that the increased power in the 10 to 20-year band and decreased power at lower frequency seen in Fig. 4 for $\Delta T$ is essentially a winter–spring phenomenon. The ratio of $\Delta T$ power in the 10 to 20-year band to that contained in periods longer than 50 years exceeds a factor 3 for the period January through May, and is largest in late winter—not shown. This goes in hand with the large squared coherence between $T_N$ and $T_S$ in the 10 to 15-year band during these months (not shown). Interestingly, a similar increase of power in the 10 to 20-year band, relative to the low-frequency tail of the GIL spectrum, is only found in late winter (February, March, April). It is during this period of the year that the strength of the $T_N/T_S$ dipole is the largest (strongest negative covariance between $T_N$ and $T_S$). This suggests that two-way interactions between $\Delta T$ and the GIL are the strongest in late winter.

## 5. THEORETICAL INTERPRETATION

A passive response of the intergyre gyre to stochastic NAO forcing (no feedback of SST anomaly on the surface winds) could introduce decadal variability in SST near the western boundary, as suggested by various theoretical studies (Frankignoul *et al.* 1997; Jin 1997). We will thus consider this scenario as a likely candidate to explain the pronounced decadal variability seen in $\Delta T$ (section 5(a)(i)). Nevertheless, two of our observational findings lead us to emphasize the possible role of ocean–atmosphere coupling. First, we note the remarkably strong coherence found between $T_N$ and $T_S$ in the 10 to 15-year band (stronger than in all other frequency bands, see Fig. 5), and its related broad-band peak seen in the $\Delta T$ index. Such a frequency dependence is striking and, to be consistent with a passive gyral response theory, would require a strong zonal dependence of the surface wind-stress forcing (Jin 1997), which is not supported by our analysis (Fig. 7(b)). Second, we observe that the spectral structure seen in the $\Delta T$ index imprints on the SLP composite power spectrum (Fig. 11). In section 5(a)(ii), using the theoretical framework developed by Marshall *et al.* (2001a), we interpret these features as a result of a strongly damped oscillation between the state of the midlatitude wind-driven ocean circulation and that of the surface atmospheric circulation.

### (a) *A model for the decadal evolution of $\Delta T$*

We assume that the time evolution of the $\Delta T$ index is governed by turbulent surface heat exchange (latent + sensible) and advection by geostrophic currents. Accordingly, we write an evolution equation for $\Delta T$ as

$$\frac{\mathrm{d}\Delta T}{\mathrm{d}t} = -\lambda \Delta T - \alpha N + Q_o \tag{2}$$

where $Q_o$ represents advection of heat by ocean circulation from one side of the Gulf Stream to the other (the northern and southern boxes of Fig. 1) and $\lambda^{-1}$ denotes a damping time-scale for $\Delta T$ due to air–sea interaction. The stochastic turbulent surface heat flux governed by the SLP composite is represented by $\alpha N$, where the parameter $\alpha > 0$ scales the stochastic component of the surface wind-stress $N$ into a surface heat-flux anomaly*, assuming the following linear model for surface wind-stress anomalies

* This term may also include forcing by Ekman advection as the latter has the same large-scale pattern (with the same sign) as that of the surface turbulent heat flux (not shown).

$\tau$ associated with the SLP composite,

$$\tau = N - f\Delta T. \tag{3}$$

Here $\tau$ represents the difference between anomalous westerlies and trade winds ($\tau > 0$ means stronger westerlies and trades winds, and implies cooling (warming) north (south) of the Gulf Stream). The possible effects of coupling are represented by the SST dipole feedback $f$ on $\tau$. Both observations (Czaja and Frankignoul, personal communication) and the response of atmospheric general-circulation models to prescribed SST, suggest that $f$ is small and positive (e.g. Rodwell *et al.* 1999; Watanabe and Kimoto 2000), i.e. that $\Delta T$anomalies tend to reinforce the anomalous wind which, to zero order, have generated them. As discussed by Marshall *et al.* (2001a), this empirical parametrization is a crude representation of how the surface baroclinicity, as measured by $\Delta T$, may interact with the Atlantic storm track and impact the NAO.

$Q_o$ represents the heating rate due to anomalous advection of heat by the wind-driven intergyre gyre discussed in section 4(a)(ii). The emphasis on anomalous currents acting on mean SST gradient rather than mean currents acting on anomalous SST gradient (i.e. $v'\overline{T}$ rather than $\overline{v}T'$) is motivated by the fact that the $T_N$ and $T_S$ boxes lie on either side of, rather than along, the separated Gulf Stream and its extension.

We interpret Eqs. (2) and (3) as dimensionless (see appendix B for a derivation of the non-dimensional equations), and we use linear Sverdrup dynamics to relate $Q_o$ to $\tau$ (see Marshall *et al.* (2001a)):

$$Q_o = g \int_{t-t_d}^{t} \tau \, dt \tag{4}$$

expressing that increased westerlies and trade winds ($\tau > 0$) yield, with some delay $t_d$, an anticyclonic ($\psi_g > 0$) circulation of the intergyre gyre. The efficiency of this gyre in carrying heat across the mean path of the separated Gulf Stream is measured by the parameter $g$ (an estimate of $g$ is provided in appendix B). The delay $t_d$ is related to the time it takes for the first baroclinic Rossby waves to spin-up the intergyre gyre. Based on the estimates of the first baroclinic Rossby-wave phase speed $c$ by Killworth *et al.* (1997; their Fig. 7), the delay is $\sim 4$ years at 30°N ($c = 3$ cm s$^{-1}$) at the southern rim of the intergyre gyre, and $\sim$12 years at 40°N ($c = 1$ cm s$^{-1}$), roughly the mean latitude of the intergyre gyre, assuming a zonal length-scale $L_x \simeq 3000$ km. The delay is even longer in the northern part of the intergyre gyre. In the following, we will choose a reference estimate of $t_d = 10$ years.

When $Q_o$ in (2) is set to zero, (2) is the same as the archetypal stochastic climate model of FH77. This model predicts an exponential decay of $\Delta T$ anomalies (with a decorrelation time-scale of $\lambda^{-1}$), and may be thought of as the continuous version of the AR(1) model used in section 3(c). When $Q_o \neq 0$, we consider two limit cases. In the first, the passive gyre, we set $f = 0$ in (3) and stochastically force $Q_o$ with $N = \tau$. This will capture the essence of the structure seen in the observed $\Delta T$ power. In the second, the gyre with feedback, we allow feedback of $\Delta T$ on $\tau$ ($f \neq 0$ in (3)). This will allow the ocean circulation to impact the atmosphere, via $\Delta T$, and will offer a better comparison with the observations.

(i) *'Passive' gyre.* If we neglect the small feedback of $\Delta T$ on the surface wind-stress, then the wind-driven component of $Q_o$ represents the forced response of the intergyre gyre to the natural variability of the surface winds. Using (3) and (4), and scaling time

by $t_d$, one obtains, if $f = 0$,

$$Q_o = g \int_{t-1}^{t} N \, dt. \tag{5}$$

The impact of $Q_o$ onto the $\Delta T$ evolution (2) is then simply to add another stochastic forcing term to $-\alpha N$, although one which is much more persistent. Because $Q_o$ as modelled by (5), and the local surface forcing $-\alpha N$ are not uncorrelated, the power spectrum of $\Delta T$ implied by this model is not simply the superposition of the two forcing spectra. We see from (5) that on time-scales longer than the spin-up time of the intergyre gyre $Q_o \simeq gN$, so that the prediction for the low-frequency energy level $F_{\Delta T}(0)$ of the $\Delta T$ power spectrum is

$$F_{\Delta T}(0) = \frac{(\alpha - g)^2}{\lambda^2} F_N(0) \tag{6}$$

where $F_N(0)$ denotes the low-frequency energy level of $N$. At very low frequency the two stochastic forcings (surface heat exchange and advection) tend to compensate one another: the level of the 'white noise' forcing, $(g - \alpha)N$, is *reduced* compared with the case of no ocean circulation ($g = 0$). A rough estimate of $g$ and $\alpha$ is provided in appendix B; they are found to be of similar magnitude ($\alpha \simeq 2.5g$), in agreement with the previous discussion of the relative magnitude of the intergyre gyre heat transport and the local surface heat flux (section 4(a)(ii)). We emphasize that this notable signature of ocean dynamics is due to the different sign of the local (surface forcing) and remote (ocean advection) equilibrium response of $\Delta T$ to the same large-scale pattern of anomalous atmospheric circulation. If we had assumed that the equilibrium response of the intergyre gyre to increased westerlies and trade winds was to transport heat from the northern to the southern side of the Gulf Stream, then the local and remote response would have added together at low frequency increasing the power of $\Delta T$ compared with the case when ocean circulation is absent.

(ii) *Gyre with feedback.* If we now neglect the forced response of the intergyre gyre to $N$, but retain its response to $\Delta T$-induced surface winds, then our model for $Q_o$ becomes

$$Q_o = -g \int_{t-1}^{t} f \Delta T \, dt \simeq -fg \Delta T(t - 1/2) \tag{7}$$

where the integral has been approximated by a midpoint value. When (7) is used in (2), then the $\Delta T$ evolution equation has the form of a stochastically forced delayed oscillator model. It has been studied in great detail by Marshall *et al.* (2001a) (see also Czaja and Marshall (2000)). They show that for a realistic regime of parameters, (2) and (7) produce damped oscillations. The gravest mode of oscillation has a frequency $\omega_0$, primarily set by the delay $t_d$ ($\omega_0$ is slightly smaller than $2\pi/t_d$). This oscillation is fundamentally of coupled origin (it requires $f \neq 0$) and bears some similarity with the hypothesis put forward by Latif and Barnett (1994) in the North Pacific (see section 6).

The gyre with feedback model also predicts a decrease of power for $\Delta T$ on long time-scales, as the ocean circulation modelled by (7) acts as an additional damping on $\Delta T$ at low frequency ($\omega \ll \omega_0$). Indeed, the low-frequency energy level of $\Delta T$ is found to be, using (7) in (2)

$$F_{\Delta T}(0) = \frac{\alpha^2}{(\lambda + fg)^2} F_N(0) \tag{8}$$

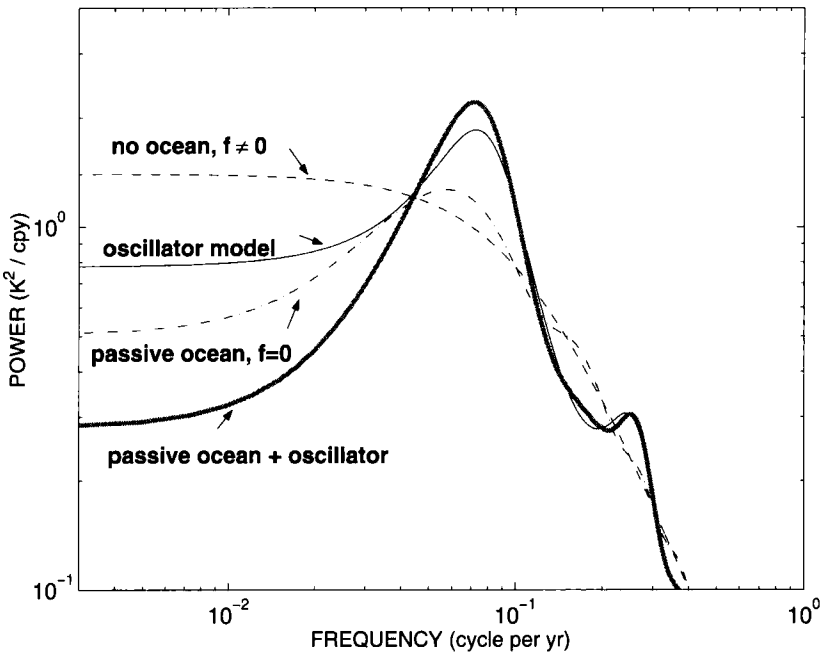


Figure 13. $\Delta T$ power spectrum predictions (see text) for the Frankignoul and Hasselmann (1977) model (dashed line), the passive gyre model (dotted-dashed line), the delayed oscillator model (thin continuous line), and the combination of passive gyre and feedback (thick continuous line). The frequency assumes a time delay of 10 years.

which indicates a lower energy level compared with FH77 ($g = 0$) if, as we have assumed $fg > 0$ (an increased SST gradient across the Gulf Stream impacts a positive phase of the NAO, i.e. $f > 0$, and the intergyre gyre acts as a delayed negative feedback, i.e. $g > 0$).

(iii) *Full model.* Figure 13 compares the various predictions for the $\Delta T$ power spectrum. Compared with FH77, both the passive gyre and the gyre with feedback models predict a decrease of power at time-scales longer than $t_d$, as discussed above. The latter is the most pronounced for the full model, when both the stochastic and $\Delta T$-induced wind stress force the intergyre gyre (using (2), (3) and (4)). On decadal time-scales, it is only when coupling is considered that the predictions significantly differ from FH77. This is related to the existence of the coupled oscillation at $\omega = \omega_0$, which is excited by the stochastic atmospheric forcing.

When coupling is considered, the structures seen in the power spectrum of $\Delta T$ can imprint back on the atmosphere. Figure 14 shows the model predictions for the power spectrum of $\tau$. First we remind the reader of the simpler case when no ocean circulation is considered ($Q_o = 0$ in (2)), but when coupling is allowed to modulate the atmospheric power spectrum in the FH77 model, as studied by Barsugli and Battisti (1998). If $f > 0$, one observes an increase of power in $\tau$ at periods longer than the damping time-scale $\lambda^{-1}$ (Fig. 14). Now, taking into account the ocean circulation ($Q_o$ modelled by (7)), we see a distinct signature on the power spectrum of $\tau$. Compared with the previous case, $\tau$ has a reduced power at low frequency and a peak near $\omega_0$, consistent with the signatures predicted by the gyre with feedback and full models for $\Delta T$ (Fig. 13). When no coupling is considered, $\tau$ is simply a white noise, with a constant spectral density.

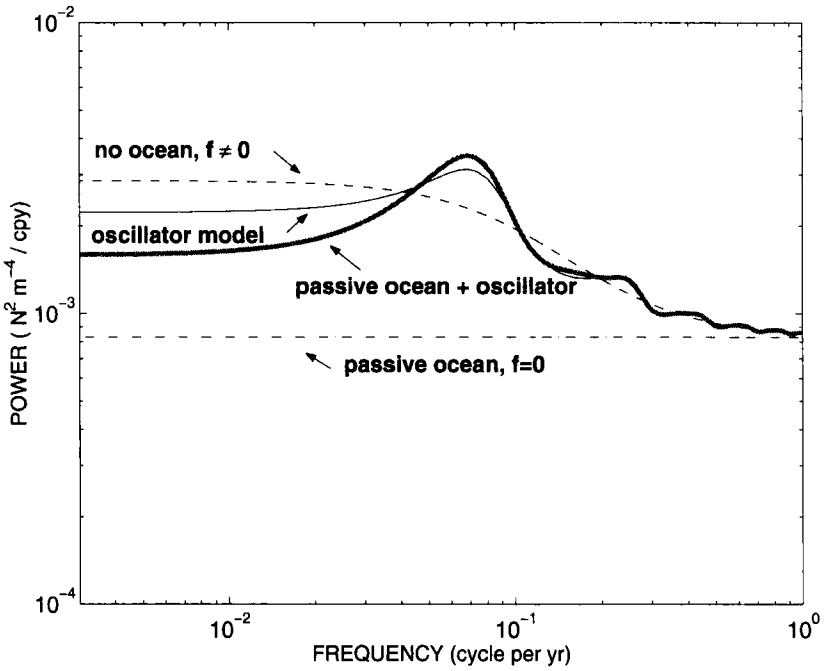


Figure 14. Same as Fig. 13 but for the surface wind-stress $\tau$ as modelled by Eq. (3).

### (*b*) *Comparison with the observations*

To make quantitative predictions, we need an estimate of the low-frequency energy level of the stochastic forcing $F_N(0)$. This is obtained by computing the monthly variance $\sigma_\tau^2$ of $\tau$ from the recent observations (using the NCEP–NCAR reanalysis over the period 1958–98 yields $\sigma_\tau^2 = (0.1)^2\ \mathrm{N^2m^{-4}}$), and assuming a white spectrum for the latter. The net result is a rough estimate of $F_N(0) = 8.3 \times 10^{-4}\ \mathrm{N^2m^{-4}}$ per cpy, used in the model predictions for $\tau$ when no feedback with $\Delta T$ is considered ($f = 0$, Fig. 14). In the following, we will compare the observed SLP power spectra shown in Fig. 11 with the model predictions for $\tau$, because a long observational record of the surface wind pattern associated with the $\Delta T$index is not available.

Let us first compare the predicted $\Delta T$ spectra (Fig. 13) with the observations (Fig. 4). It is seen that the choice of $t_\mathrm{d} = 10$ years provides a reasonable fit to the broad-band peak seen in the observed $\Delta T$ index in the 10 to 20-year band. Furthermore, to account for the energy level of $\Delta T$ in that frequency band, it is necessary to invoke coupling as the predictions from the passive gyre or FH77 models are too small by a factor two in the 10 to 20-year band. At longer time-scales, the passive gyre model gives the best predictions for $F_{\Delta T}(0)$, as the full model overestimates the latter by about a factor two.

Clearly the SLP observations (Fig. 11), which are a proxy for surface wind fluctuations, deviate from a white noise power spectrum. Consequently, the predictions of the passive gyre case (white atmospheric spectra, Fig. 14) differ from the observations: they do not reproduce the broad-band peak near 10–20 years seen in the GIL power spectrum and its subsequent decrease of power on longer time-scales. Neither do they reproduce the increase of power with time-scale seen in the STH spectrum. On the other hand, the GIL power spectrum is consistent with the full model for $\tau$ (including feedback, Fig. 14),

which predicts a ratio of power in the decadal (10–20 year) to the very-low-frequency band (periods longer than 50 years) of 2 compared to 3 in the observations.

Note that a small feedback $f$ is needed to predict the GIL spectrum. As shown in appendix B, we use $f \sim 0.015$ (N m$^{-2}$) K$^{-1}$, implying that a large $\Delta T$ anomaly of 1 K is only associated with a surface wind change of 0.015 N m$^{-2}$, roughly 15% of the observed standard deviation of $\tau$. Another way to express the feedback is in terms of the SLP anomaly. Using the geostrophic relation to express the surface wind amplitude $|U|$ in terms of the SLP anomaly, and assuming $\tau \simeq \rho C_D |U|^2$ (where $\rho = 1.2$ kg m$^{-3}$ is the surface air density, and $C_D = 4 \times 10^{-3}$ is a drag coefficient), one finds that a surface wind-stress anomaly of 0.015 N m$^{-2}$ is equivalent to a pressure fluctuation of 1–2 mb with a length-scale of about 1000 km. Once again it is seen that the required feedback is small (1–2 mb K$^{-1}$). For this value of $f$, it is found that the quality factor $q$ of the oscillations predicted by the gyre with feedback model (see Czaja and Marshall (2000)) is small ($q \simeq 2$). With a $q$ factor of 2, given an initial condition, $\Delta T$ diminishes in amplitude, changes sign after a few years, and then shows no more significant signals. This is in very good agreement with the observed SST composite (Fig. 3).

The different structure seen in the GIL spectrum and that of the NAO or SLP anomaly near the STH region (the southern centre of action of the NAO) at low frequency (periods longer than 25 years) is intriguing. It is not consistent with our theory which would predict a decrease of power for the whole NAO pattern. This suggests that, in late winter, factors other than $\Delta T$/storm-track dynamics control the strength of the SLP anomaly over the STH region at these long time-scales.

## 6. Discussion and comparison with previous studies

Our analysis of the observations has connections to that of Deser and Blackmon (1993), although we use simpler techniques and a longer dataset. In agreement with the result of their EOF analysis (their 'dipole mode'), we showed evidence for a pronounced decadal time-scale in the variability of North Atlantic SST. Both Deser and Blackmon's second SST principal component (PC2) and the $\Delta T$ index introduced here, show a broad-band peak in the 10 to 20-year band, as expected from the similarity between our SST index (SST difference across the separated Gulf Stream) and their 2nd EOF pattern. However, the power spectra of the two indices differ at time-scales longer than about 25 years: whereas $\Delta T$ shows decreasing power on longer time-scales (Fig. 4), Deser and Blackmon's PC2 shows the opposite trend (their Fig. 3(a)). The different datasets used in the two studies (COADS vs. Kaplan) may be a possible explanation. However, we find that the power spectrum of the 1st EOF of North Atlantic SST in winter, obtained using the Kaplan *et al.* (1997) reanalysis, shows a similar power spectrum to that of the second EOF in Deser and Blackmon (1993), and a very similar pattern (the tripole). This suggests that the difference in the power spectra is likely to stem from the differing measures of SST variability. The EOF analysis employed by Deser and Blackmon emphasizes large-scale pattern and reflects SST variability outside the Gulf Stream region; the analysis here considers the difference in SST across the Gulf Stream. Our analysis also reveals a similar spectral feature present in the SLP anomaly in the GIL region (Fig. 11), which remains coherent with $\Delta T$ at these long time-scales (Fig. 12). The use of a longer dataset in our study (143 years instead of 90 years) also certainly allows a better, although still limited, investigation of these long time-scales.

Along with our analysis of data, we have proposed a possible mechanism that can account for the features seen in our spectra (section 5). A broad spectral peak could be

the result of anomalous advection of heat by the intergyre gyre, which, on long time-scales, partially cancels the local surface forcing of $\Delta T$ by air–sea fluxes. We note that the tendency for Atlantic SST anomalies to expand out to basin scale at interdecadal time-scales (Kushnir 1994) may also be a factor explaining the decrease of power seen in $\Delta T$, possibly related to slow changes in overturning circulation over the North Atlantic (Delworth and Mann 2000). This effect is hinted at in Fig. 5, where $T_N$ and $T_S$ become in phase at the longest time-scales resolved.

In summary, the delayed oscillator framework of Marshall *et al.* (2001a), used here to interpret the observations, is in accord with the scenario proposed by Grötzner *et al.* (1998) to explain the decadal variability seen in a long integration of a coupled atmosphere–ocean model. There is nevertheless a major difference in that Grötzner *et al.* (1998) argue for an unstable coupled atmosphere–ocean oscillation, whereas we emphasize that the oscillation is heavily damped (we estimated the quality factor to be about 2, see appendix B). In favour of the interpretation set out here, we note that there is observational evidence that air–sea interactions act to damp SST anomalies in the North Atlantic sector (Frankignoul *et al.* 1998; see also Czaja and Frankignoul 1999).

## 7. Conclusions

We have presented observations based on a simple index of SST variability, $\Delta T$, and its covarying atmospheric pattern, that reveals non trivial air–sea interaction over the Atlantic sector. A broad-band peak in the 10 to 20-year band is seen on the $\Delta T$ power spectrum, with a subsequent decrease of power as one goes to longer periods. We have argued that on decadal time-scales, SST variations across the separated Gulf Stream are largely controlled by anomalous ocean currents which in turn modulate the low-frequency evolution of a dipolar SLP pattern, with centres of action over the Greenland–Iceland and the STH regions. The power spectrum of this SLP pattern, and particularly its northern centre of action (Greenland–Iceland), also shows a broad-band peak near a 10 to 20-year period, and a continuous decrease of power on longer time-scales. The SST anomalies captured by the $\Delta T$ index extend to the subtropical region of the North Atlantic, which is primarily a result of the large-scale surface forcing coordinated by the atmosphere.

We have outlined a possible theoretical interpretation, by including a simple representation of anomalous ocean advection and atmosphere–ocean coupling into the archetypal model of FH77. The main result obtained from the model is that the ocean response to the NAO surface forcing has to act as a delayed negative feedback in order to reproduce the low-frequency decrease of power seen in the observed $\Delta T$. We have emphasized the role of wind-driven anomalous ocean currents (the 'intergyre' gyre of Marshall *et al.* 2001a) in providing a possible mechanism. We have argued that the particular configuration of the mean SST gradient and anomalous NAO wind-stress curl may favour an anomalous heat transport across the separated Gulf Stream axis, so that the wind-driven ocean response to the NAO partially compensates the thermal impact of the NAO at the surface at long time-scales. Note that the thermohaline response of the ocean to the NAO forcing (dipolar buoyancy forcing across the separated Gulf Stream axis) can also be invoked to compensate the buoyancy loss/gain by across Gulf Stream heat transport, and is one of the scenarios discussed by Marshall *et al.* (2001a). A different, although related, perspective on the role of thermohaline processes is given by Delworth and Mann (2000), who suggest that SST anomalies of basin-scale might be generated on an interdecadal time-scale as a result of intrinsic fluctuations of the North Atlantic overturning circulation. If this process is strong enough to dominate over local

surface forcing associated with the NAO (which generates dipolar SST anomalies north and south of the separated Gulf Stream) it may reduce the strength of the $\Delta T$ index on interdecadal time-scales, as seen in the observations. Clearly, more study is needed to elucidate the relative importance of wind vs. thermohaline processes. Idealized numerical experiments (Herbaut *et al.* 2001) suggest that the two add constructively with similar time-scales (5–10 years) and amplitude, but this is less clear in more sophisticated models (Eden and Willebrandt 2001).

We showed that allowing some feedback of $\Delta T$ onto the atmospheric circulation may peak the power spectrum of both $\Delta T$ and its related pattern of surface winds in the decadal band, in agreement with the observations. This does not require a strong feedback of $\Delta T$ on the surface winds (we assumed $f \simeq 0.015$ (N m$^{-2}$) K$^{-1}$, or equivalently $f \simeq 1 - 2$ mb K$^{-1}$), because the strong SST gradients near the western boundary enable an anomalous ocean circulation to carry a large quantity of heat into the mixed layer. The suggestion that the strength of the GIL may be partially controlled by anomalous ocean heat transport at decadal and longer time-scales has to be tested further in coupled simulations.

## ACKNOWLEDGEMENTS

It is a pleasure to acknowledge Carl Wunsch for several stimulating discussions and his help at various stages of this study. The authors were supported by a grant from the CLIVAR Atlantic program of the Office of Global Programs of the National Oceanic and Atmospheric Administration.

## APPENDIX A

### *Heat transport of the intergyre gyre*

To estimate how much heat is carried by the intergyre gyre from the southern ($T_S$) to the northern ($T_N$) box, north and south of the separated Gulf Stream (see Fig. 1), we estimate how much heat it transports across the climatological zero wind-stress-curl line (hereafter ZWCL). The intergyre gyre straddles the mean position of the ZWCL (Fig. 8). The climatological mean SST decreases along the zero curl line and so, if the integyre gyre has anticyclonic sense, it carries warm water polewards and cold water equatorward across it (and vice versa). However, only a fraction of the intergyre gyre mass transport occurs in the mixed layer (of depth $h$). Assuming that the total intergyre gyre mass transport is roughly constant over the thermocline (of depth $H$) and zero below, we scale the heat transport $H_{ig}$ of the intergyre gyre according to

$$H_{ig} \simeq \rho_0 C_p \Psi_{ig|w} \delta\overline{T} \frac{h}{H} \tag{A.1}$$

where $C_p$ is the specific heat of sea water at constant pressure, $\Psi_{ig|w}$ denotes the typical amplitude of the intergyre gyre mass transport (evaluated just inside the western boundary current) and $\delta\overline{T}$ denotes the climatological SST variation along the ZWCL. From (A.1) we see that the efficiency of the intergyre gyre in carrying heat across the ZWCL depends on (i) a non-zero anomalous stream function along the ZWCL, i.e. it requires that the anomalous wind-stress-curl forcing straddles the climatological mean wind-stress curl, and (ii) climatological SST variations along the ZWCL. Because $\Psi_{ig|w}$ evolves on a longer time-scale than the seasonal cycle, $\delta\overline{T}$ is chosen to be the climatological annual mean SST change along the ZWCL. Note, however, that $\delta\overline{T}$ has

a pronounced seasonal cycle, being larger in summer and weaker in winter (not shown). Inserting typical numbers ($\Psi_{ig|w} = 10$ Sv; $\delta\overline{T} = 4$ K see Fig. 1; $h = 100$ m; $H = 600$ m) one finds $H_{ig} \simeq 25$ TW.

## APPENDIX B

### *Non-dimensional model equations and estimation of the model parameters*

We start with the dimensional equations for $\Delta T$ and $\tau$ for the case of purely wind-driven oceanic effects (we refer the reader to Marshall *et al.* (2001a) for the discussion and derivation of the meridional overturning model)

$$\frac{\mathrm{d}\Delta T}{\mathrm{d}t} = -\lambda\Delta T - \alpha N + g\psi_g \tag{B.1}$$

$$\tau = N - f\Delta T. \tag{B.2}$$

Following Marshall *et al.* (2001a), we model the intergyre gyre stream function according to time-dependent Sverdrup dynamics. Using the same simplified analytical formula for the spatial pattern associated with $\tau$ (only latitude dependent, their Eq. (47)) and similar scaling for the zonal and meridional scales ($L_x = L_y \simeq 3000$ km), surface wind ($\tau_{wind} = 0.05$ N m$^{-2}$), gyre strength ($\Psi_G = L_x \pi \tau_{wind}(\rho L_y \beta)^{-1} \simeq 10^7$ m$^3$s$^{-1} = 10$ Sv, and time ($t_d = L_x c^{-1} \simeq 10$ years) one can show that (see Marshall *et al.* (2001a) for a complete derivation)

$$\psi_g = \int_{t-1}^{t} \tau \, \mathrm{d}t. \tag{B.3}$$

Scaling $N$ by $\tau_{wind}$ and $\Delta T$ by $\Upsilon = 1$ K, the non-dimensional form of (B.1) and (B.2) become ($\Delta T$, $\tau$, $N$ and $\psi_g$ are now non-dimensional)

$$\frac{\mathrm{d}\Delta T}{\mathrm{d}t} = -\lambda t_d \Delta T - \frac{\alpha t_d \tau_{wind}}{\Upsilon} N + \frac{g t_d \Psi_G}{\Upsilon}\psi_g \tag{B.4}$$

$$\tau = N - \frac{f\Upsilon}{\tau_{wind}}\Delta T \tag{B.5}$$

which with (B.3) defines the model used for the predictions of section 5(b).

The non-dimensional model parameters (denoted by a star) are then $\lambda^* = \lambda t_d$, $\alpha^* = \alpha t_d \tau_{wind} \Upsilon^{-1}$, $g^* = g t_d \Psi_G \Upsilon^{-1}$ and $f^* = f \Upsilon \tau_{wind}^{-1}$. Assuming a typical damping time-scale of about a year, we set $\lambda^* = 7$.

We estimate $\alpha^*$ empirically from monthly data. Using the NCEP–NCAR reanalysis we computed an averaged time series of monthly anomalies of surface turbulent heat flux and surface wind stress in regions of strong correlation with $\Delta T$ (roughly the $T_N$ and $T_S$ boxes). The regression of wind stress onto the heat flux time series in winter provides a rough estimate of $\rho C_p h\alpha \simeq 5 \times 10^2$ W m$^{-2}$ per N m$^{-2}$, which then implies $\alpha^* \simeq 20$.

We use the estimate of the heat transport of the intergyre gyre developed in appendix A to estimate $g^*$. First we relate $H_{ig}$ to the wind-driven component of $Q_o = g\psi_g$ from the heat budget of the northern and southern boxes. When the northern box gains heat at a rate $H_{ig}(\rho C_p h A)^{-1}$, where $A$ denotes the typical area of the northern and southern boxes ($A \simeq 4 \times 10^{12}$ m$^{-2}$), the southern box looses heat at a rate

$-H_{ig}(\rho C_p h A)^{-1}$. Thus, the difference, $\Delta T$, is driven by $Q_o = 2H_{ig}(\rho C_p h A)^{-1}$. Inserting (A.1) in the latter equation and identifying $\psi_g$ to $\Psi_{ig|w}$ one gets

$$g = \frac{2\delta\overline{T}}{AH}. \tag{B.6}$$

The value for $g^\star$ is then found to be $g^\star \simeq 8$. Finally, assuming a dimensional feedback $f = 0.015$ (N m$^{-2}$) K$^{-1}$ we have $f^\star \simeq 0.3$.

For these parameters, the critical number $R = f^\star g^\star (\lambda^\star)^{-1}$ of the delayed oscillator model (2)–(7) (see Marshall *et al.* (2001a)) is found to be $R \simeq 0.4$. This is associated with strongly damped free modes. If one defines the quality factor, $q$, of these damped oscillations as the ratio of their frequency to their inverse damping time-scale, then the gravest mode has a $q$ of $\sim$2 (see Czaja and Marshall (2000)).

## REFERENCES


Amos, D. E. and Koopmans, L. H. 1963 Tables of the distribution of the coefficient of coherence for stationary bivariate Gaussian processes. Sandia Corporation monograph

Barsugli, J. J. and Battisti, D. S. 1998 The basic effects of atmosphere–ocean thermal coupling on mid-latitude variability. *J. Atmos. Sci.*, **55**, 477–493

Battisti, D. S., Bhatt, U. S. and Alexander, M. A. 1995 A modeling study of the interannual variability of the North Atlantic Ocean. *J. Climate*, **8**, 3067–3083

Bjerknes, J. 1964 Atlantic air–sea interaction. *Adv. Geophys.*, **10**, 1–82, Academic Press

Box, G. E. P., Jenkins, G. M. and Reinsel, G. C. 1994 *Time series analysis: forecasting and control.* Prentice-Hall, 3rd edition

Cayan, D. 1992 Latent and sensible heat flux anomalies over the northern oceans: driving the sea surface temperature. *J. Phys. Oceanogr.*, **22**, 859–881

Czaja, A. and Frankignoul, C. 1999 Influence of the North Atlantic SST anomalies on the atmospheric circulation. *Geophys. Res. Lett.*, **26**, 2969–2972

Czaja, A. and Marshall, J. 2000 On the interpretation of AGCMs response to prescribed time varying SST anomalies. *Geophys. Res. Lett.*, **27**, 1927–1930

Delworth, T. L. and Mann, M. E. 2000 Observed and simulated multi-decadal variability in the northern hemisphere. *Clim. Dyn.*, **16**, 661–676

Deser, C. and Blackmon, M. L. 1993 Surface climate variations over the North Atlantic Ocean during winter: 1900–1989. *J. Climate*, **6**, 1743–1753

Eden, C. and Willebrandt, J. 2001 Mechanism of interannual to decadal variability of the North Atlantic circulation. *J. Climate*, in press

Frankignoul, C. and Hasselmann, K. 1977 Stochastic climate models. Part II: Application to sea-surface temperature variability and thermocline variability. *Tellus*, **29**, 289–305

Frankignoul, C., Müller, P. and Zorita, E. 1997 A simple model of the decadal response of the ocean to stochastic wind forcing. *J. Phys. Oceanogr.*, **27**, 1533–1546

Frankignoul, C., Czaja, A. and L'Hévéder, B. 1998 Air–sea feedback in the North Atlantic and surface boundary conditions for ocean models. *J. Climate*, **11**, 2310–2324

Grötzner, A., Latif, M. and Barnett, T. P. 1998 A decadal climate cycle in the North Atlantic Ocean as simulated by the ECHO coupled GCM. *J. Climate*, **11**, 831–847

Halliwell, G. 1998 Simulation of North Atlantic decadal/multidecadal winter SST anomalies driven by basin-scale atmospheric circulation anomalies. *J. Phys. Oceanogr.*, **28**, 5–21

Herbaut, C., Sirven, J. and Czaja, A. 2001 An idealized model study of the mass and heat transports between the subpolar and subtropical gyres. *J. Phys. Oceanogr.*, in press

Hurrell, J. 1995 Decadal trends in the North Atlantic Oscillation: regional temperatures and precipitation. *Science*, **269**, 676–679

Hurrell, J. and Trenberth, K. E. 1999 Global sea surface temperature analyses: multiple problems and their implications for climate analysis, modeling, and reanalysis. *Bull. Am. Meteorol. Soc.*, **80**, 2661–2678

Jin, F. 1997 A theory of interdecadal climate variability of the North Pacific ocean–atmosphere system. *J. Climate*, **10**, 1821–1835

Kalnay, E. *et al.* 1996 The NCEP/NCAR 40-year reanalysis project. *Bull. Am. Meteorol. Soc.*, **103,** 18567–18589

Kaplan, A., Kushnir, Y., Cane, M. and Blumenthal, B. 1997 Reduced space optimal analysis for historical datasets: 136 years of Atlantic sea surface temperatures. *J. Geophys. Res.*, **102,** 27835–27860

Kaplan, A., Kushnir, Y. and Cane, M. A. 2000 Reduced space optimal interpolation of historical marine sea level pressure: 1854–1992. *J. Climate*, **13,** 2987–3002

Killworth, P. D., Chelton, D. B. and De Szoeke, R. A. 1997 The speed of observed and theoretical long extratropical planetary waves. *J. Phys. Oceanogr.*, **27,** 1946–1966

Kushnir, Y. 1994 Interdecadal variations in North Atlantic sea surface temperature and associated atmospheric conditions. *J. Climate*, **7,** 141–157

Latif, M. and Barnett, T. P. 1994 Causes of decadal climate variability in the North Pacific/North Atlantic sector. *Science*, **266,** 634–637

Mann, M. E. and Park, J. 1994 Global scale modes of surface temperature variability on inter-annual to century timescales. *J. Geophys. Res.*, **99,** 25819–25833

Marshall, J., Johnson, H. and Goodman, J. 2001a A study of the interaction of the North Atlantic Oscillation with the ocean circulation. *J. Climate*, **14,** 1399–1421

Marshall, J., Kushnir, Y., Battisti, D., Chang, P., Czaja, A., Hurrell, J., McCartney, M., Saravanan, R. and Visbeck, M. 2001b Atlantic climate variability: Phenomena, impacts and mechanisms. *Int. J. Climatol.*, in press

Percival, D. B. and Walden, T. A. 1993 *Spectral analysis for physical applications. Multitaper and conventional univariate techniques.* Cambridge University Press

Rodwell, M. J., Rowell, D. P. and Folland, C. K. 1999 Oceanic forcing of the wintertime North Atlantic Oscillation and European climate. *Nature*, **398,** 320–323

Saravanan, R., Danabasoglu, G., Doney, S. C. and McWilliams, J. C. 2000 Decadal variability and predictability in the midlatitude ocean–atmosphere system. *J. Climate*, **13,** 1073–1097

Sutton, R. T. and Allen, M. R. 1997 Decadal predictability of North Atlantic sea surface temperature and climate. *Nature*, **388,** 563–567

Tourre, Y. M., Rajagolapan, B. and Kushnir, Y. 1999 Dominant patterns of climate variability in the Atlantic Ocean during the last 136 years. *J. Climate*, **12,** 2285–2299

Trenberth, K. E. and Paolino, D. A. 1980 The northern hemisphere sea-level pressure data set: trends, errors and discontinuities. *Mon. Weather Rev.*, **108,** 855–872

Watanabe, M. and Kimoto, M. 2000 Atmosphere–ocean thermal coupling in the North Atlantic: A positive feedback. *Q. J. R. Meteorol. Soc.*, **126,** 3343–3369